Crystallographic Texture in Pulsed Laser Deposited Hydroxyapatite Bioceramic Coatings

Hyunbin Kim,[a] Renato P. Camata,[b] Sukbin Lee,[c] Gregory S. Rohrer,[c] Anthony D. Rollett,[c] and Yogesh K. Vohra[b]

[a] Department of Materials Science and Engineering, University of Alabama at Birmingham, Birmingham, Alabama 35294
[b] Department of Physics, University of Alabama at Birmingham, Birmingham, Alabama 35294
[c] Department of Materials Science and Engineering, Carnegie Mellon University, Pittsburgh, Pennsylvania 15213

The orientation texture of pulsed laser deposited hydroxyapatite coatings was studied by X-ray diffraction techniques. Increasing the laser energy density of the KrF excimer laser used in the deposition process from 5 to 7 J/cm^2 increases the tendency for the c-axes of the hydroxyapatite grains to be aligned perpendicular to the substrate. This preferred orientation is most pronounced when the incidence direction of the plume is normal to the substrate. Orientation texture of the hydroxyapatite grains in the coatings is associated with the highly directional and energetic nature of the ablation plume. Anisotropic stresses, transport of hydroxyl groups, and dehydroxylation effects during deposition all seem to play important roles in the texture development.

Keywords: Hydroxyapatite; Coating; Laser deposition; Texture; Ceramics; Bone

Published as:
H. Kim, R.P. Camata, S. Lee, G.S. Rohrer, A.D. Rollett, Y.K. Vohra, "Crystallographic Texture in Pulsed Laser Deposited Hydroxyapatite Bioceramic Coatings," Acta Materialia **55** (2007) 131-139.

1. Introduction

Crystallographic texture is one of the essential microstructural features that determine the properties of polycrystalline materials. Texture formation and its effect on materials properties have been extensively studied in metals [1–3] and geological materials [4–6] since the late 1940's when the introduction of pole-figure goniometers allowed the use of x-ray diffraction as a quantitative tool in the determination of orientation distributions in polycrystals [7]. A growing literature exists as well in texturing of bulk and thin film ceramics as these systems have gained greater technological importance over the past decade [8–14]. Evaluation of the effect of crystallographic texture in complex ceramics with tetragonal, orthorhombic and rhombohedral symmetries has also been a source of intense investigations recently due to the important applications of piezoelectric [15,16], ferroelectric [17,18] and thermoelectric materials [19–21]. Much less attention has been given, however, to texturing in biologically derived and biologically relevant ceramics, often referred to as bioceramics. Of particular interest in this area is the bioceramic hydroxyapatite [$Ca_{10}(PO_4)_6(OH)_2$] which constitutes the inorganic matrix of bone and tooth tissue. Naturally occurring hydroxyapatite (HA) often exhibits preferred orientations resulting from highly specific biological processes [22,23]. These textures are believed to significantly impact the biological and biomechanical performance of hard tissues [22, 24]. Texturing has also been observed in synthetic HA that is commonly coated onto metallic implants in dentistry and orthopedics to improve implant integration with adjacent bone tissue [25–27]. Despite the fact that crystallographic texture is one of the dominant features that determine the properties of polycrystalline ceramics and is

commonly observed in naturally occurring HA, its impact on the mechanical properties and bioactivity of HA-coated implants has so far received very little attention. Most of the references to preferred orientation of HA coatings in the literature are of serendipitous occurrences of texturing in coatings produced by various deposition techniques [28–31]. Efforts aimed at systematic studies and deliberate control of these orientation effects have, however, been limited. This is due in part to the experimental difficulty in controlling texture in the coatings through conventional fabrication methods. Notwithstanding these experimental challenges, recent studies indicate that unique advances in implant technology may be possible through coatings that achieve improved mechanical properties and bioactivity via preferred orientation effects [32–35]. In this study, we report how pulsed laser deposition (PLD) can be used to produce HA coatings with controlled crystallographic texture that may be relevant in implant applications and discuss the underlying processes that may be responsible for texture development in these coatings.

2. Experimental

We have produced HA coatings of thickness 1–3 μm in Ar/H_2O atmosphere by PLD using a KrF excimer laser (248 nm) with an energy density of 5–7 J/cm^2 and a pulse repetition rate of 30 Hz. The PLD setup used in our experiments is tailored after the standard HA laser deposition configuration that has been described in detail elsewhere [28, 36, 37]. The only noteworthy variant of our deposition system is the presence of a substrate holder featuring two degrees of freedom (Neocera, Beltsville, MD, USA). This system allows easy tilting of the substrate with respect to the laser plume, enabling

studies of the effect of plume direction on coating properties. The substrate was placed in the deposition system at a distance of 7.5 cm from the ablation target. The base pressure of our vacuum processing system was typically below 9×10^{-7} Torr. Deposition was carried out in an Ar/H_2O atmosphere at various pressures between 400 mTorr and 800 mTorr. Constant substrate temperatures in the range of 650–730 °C were used for deposition. The ablation targets were prepared by compressing a commercial HA powder (97.5 % purity, Plasma Biotal Ltd.) at the pressure of 2500 psi and sintered at 1200 °C in Ar/H_2O atmosphere for 1.5 hrs. Coatings were deposited on Ti-6Al-4V substrates in the form of 1 cm diameter disks prepared by polishing with SiC papers of 180 grits, 600 grits, 1200 grits, and polycrystalline diamond suspensions of 6 μm and 1 μm, and by cleaning with trichlorethylene, acetone, methanol, and deionized water in an ultrasonic bath. The Ti-6Al-4V substrates were polycrystalline with random orientation as indicated by the relative peak intensities of their 2θ X-ray diffraction scans. The phase composition of the coatings was identified using thin film X-ray diffraction (XRD) with Cu Kα radiation of 1.5418 Å wavelength with a scan speed of 0.008 °/s. Measurements of crystallographic texture were performed by XRD in reflection geometry with a standard four-circle goniometer [7]. X-ray pole figures were collected for the (0002) and $(22\bar{4}2)$ reflections of HA by varying the polar angle ranging from 0° to 85° and the azimuthal angle ranging from 0° to 360° with a step increment of 5° and a scan time of 4 s per step. The pole figures were corrected for background and defocusing of the incident beam. Background values were measured for each sample and defocusing values were adjusted using a randomly oriented HA coating. Inverse pole figures were derived from a discretized orientation distribution (OD) that was constructed by using available

measured pole figures as inputs to the WIMV algorithm in the popLA package [38]. The recalculated pole figures from the OD had the errors less than 1 % when compared with the measured pole figures. The recalculated pole figures as well as the inverse pole figures were displayed as contour plots using equal-area projection. The pole densities were normalized by that of a hypothetical sample with random orientation and are expressed in units of multiples of random distribution (MRD).

3. Results

We have studied the effect of laser energy density, plume direction of incidence, and background pressure on the crystallographic texture of polycrystalline HA coatings. Figure 1 shows XRD scans of coatings deposited at different laser energy densities. All reflections are well indexed in terms of an HA hexagonal lattice with a = 9.424 Å and c = 6.879 Å ($P6_3/m$ space group). These samples also seem to contain a small amount of CaO as indicated by a weak reflection ascribed to this material at $2\theta \approx 37.5°$. As the laser energy density increases, the reflections from high-l planes among the lattice planes (*hkil*) increase while the reflections from high-h and high-k planes decrease. This suggests formation of HA grains with the c-axis preferentially aligned in the direction perpendicular to the substrate. At the highest laser energy density investigated (7 J/cm^2), the (*hki0*) reflections of the hexagonal structure are absent from the diffraction patterns.

X-ray pole figures shown in Fig. 2 and the corresponding inverse pole figures in Fig. 3 confirm the preferential orientation of HA grains in the coatings deposited with high laser energy density. The HA $\{0001\}$ pole density in the coatings increases in the direction perpendicular to the coatings with increasing laser energy density, as seen in Fig.

2. The pole figures for the coating deposited at 5 J/cm^2 show random distribution of HA $\{0001\}$ and $\{1\bar{2}1\}$ poles with respect to the sample directions 1, 2, and 3. In the pole figures for the coating deposited at 6 J/cm^2, the HA $\{0001\}$ poles appear around the sample direction 3 which indicates the direction perpendicular to the film surface. For the coating deposited at 7 J/cm^2, the HA $\{0001\}$ poles are aligned along the direction perpendicular to the coating and the HA $\{1\bar{2}1\}$ poles are distributed around a ring at approximately 45° from the surface normal, which is in close agreement with the 45.9° angle between the $\{0001\}$ and $\{1\bar{2}1\}$ planes of HA (not discernible in the intensity scale of Fig. 2). Hence, there is a cylindrical orientation symmetry about the surface normal of the coatings, which indicates a fiber texture. The inverse pole figures shown in Fig. 3 clearly demonstrate that the density of HA $\{0001\}$ poles for the direction normal to the coatings (direction 3) increases with increasing laser energy density. This is different from the behavior observed for directions 1 and 2, which exhibit virtually no variation in pole density as a function of laser energy density. While pole figures display distribution of a specific crystal orientation with respect to the sample coordinates, inverse pole figures reveal orientation densities for a given sample direction with respect to the crystal coordinates. For the sample direction 3, there is a concentration at HA $\{0001\}$ poles in the inverse pole figures for the coating deposited at 7 J/cm^2. The density of HA $\{0001\}$ poles is reduced for the coating deposited at 6 J/cm^2. Again, the inverse pole figures for the coating deposited at 5 J/cm^2 shows no preferred orientation of HA crystallites. These are in good agreement with the observations in the pole figures. The high density of HA $\{0001\}$ poles aligned along direction 3 and the absence of any noticeable pole

alignment along the symmetric directions 1 and 2 are also indicative of the $\{0001\}$ fiber texture of HA grains in the coatings.

In order to assess the importance of the directional nature of the PLD plume in the development of texture in these coatings, we performed depositions varying the angle φ between the symmetry axis of the incident plume and the direction normal to the substrate surface as illustrated in the inset of Fig. 4. Heretofore we refer to this angle φ as the "angle of incidence" of the plume onto the substrate. In Fig. 4, we observe a change in the phase composition and crystallographic orientation of grains in the coatings as a function of the angle of incidence φ. These simple X-ray 2θ scans suggest that the highest degree of *c*-axis texturing in HA occurs for φ = 0° (i.e., normal incidence of the plume). As the angle φ increases from 0° to 45°, the reflections from high-*l* planes decrease in intensity, which indicates less *c*-axis texturing. Although qualitative in nature, these measurements may indicate that HA texture development is correlated with the direction of the energetic plume with respect to the surface. At higher values of φ, one also observes the formation of the tetracalcium phosphate [$Ca_4(PO_4)_2O$] (TTCP) phase in the coatings. TTCP, which has the monoclinic structure (a = 7.018 Å, b = 11.980 Å, c = 9.469 Å, β = 90.88°) of $P2_1$ space group, is one of the dehydrated calcium phosphate compounds. Higher values of φ apparently lead to diminished incorporation of hydroxyl groups (OH) resulting in more TTCP formation. At incidence angles of the plume higher than 30°, TTCP dominates the coatings and seems to develop its own texture with the *b*-axis of the monoclinic structure preferentially aligned perpendicularly to the substrate. This TTCP texture invariably develops, provided that enough TTCP is allowed to form in

the coatings, which requires dehydroxylation conditions during deposition (i.e., environment deficient in OH) [37].

The *c*-axis texturing of HA grains in the coatings deposited with the plume direction close to the substrate normal is demonstrated in the inverse pole figures shown in Fig. 5. The inverse pole figures for the sample direction 3 clearly show higher density of the HA $\{0001\}$ poles in the coating deposited at $\varphi = 0°$ than in the coating deposited at $\varphi = 15°$. The inverse pole figures for both coatings also reveal the $\{0001\}$ fiber texture of HA grains. As the density of HA $\{0001\}$ poles along sample direction 3 decreases ($\varphi = 15°$) the poles spread out slightly while preserving an axial symmetry about direction 3. For $\varphi > 15°$ the HA (0002) reflections overlap with the TTCP (130) reflections. The generation of HA orientation distributions in this case requires careful deconvolution of the two peaks involved, which we have not attempted in this study, and therefore inverse pole figures for $\varphi > 15°$ are not included.

Because of the critical role played by OH in HA deposition, we have also conducted experiments to assess the effect of the background pressure of Ar/H_2O, and thus OH availability, on the texturing of our coatings. Figure 6 shows simple X-ray 2θ scans from coatings deposited with various background pressures of Ar/H_2O. These coatings were deposited with a substrate temperature of 650 °C, laser energy density of 6 J/cm^2, and normal incidence of the plume. The coating obtained at a pressure of 800 mTorr contains only HA phase and appears to have random orientation. When the pressure is reduced to 700 mTorr, HA is still the only phase present in the coating but its grains seem to exhibit *c*-axis preferentially oriented along the direction normal to the substrate. At a pressure of 600 mTorr, the relative peak intensities of HA continue to

suggest *c*-axis orientation despite the presence of a small amount of CaO in the coating. This increase of the HA texturing is likely a result of the higher kinetic energy of the plume species at lower background pressure and may be associated with the same underlying mechanism of texture formation observed with increasing laser energy density. As the pressure is further reduced to 500 mTorr, a small amount of TTCP is observed in the coating (in addition to CaO already noticed at 600 mTorr). Although HA is still the main phase in the coating, the relative peak intensities of HA are now more characteristic of a randomly oriented material. The coating deposited at 400 mTorr is comprised of HA, TTCP, as well as CaO. The grains of the TTCP phase now seem to exhibit preferential orientation with the *b*-axis of their monoclinic crystal structure favoring alignment along the direction normal to the substrate. In this case a loss of HA texturing with lowering pressure below 600 mTorr seems to take place concurrently with the appearance of TTCP inclusions.

Figure 7 shows the inverse pole figures of HA in the coatings obtained at different background pressures of Ar/H_2O. In the inverse pole figures for the coating deposited at 800 mTorr, there is no concentration at any of the HA poles over the sample directions 1, 2, and 3, which indicates random orientation of HA crystallites. The inverse pole figures for the coating deposited at 700 mTorr display the concentration of the HA $\{0001\}$ poles near the sample axis 3, indicating the *c*-axis texturing along the direction perpendicular to the coating surface, in agreement with the qualitative observation noted in the 2θ scans of Fig. 6. For the coating deposited at 600 mTorr, the density of HA $\{0001\}$ poles aligned around direction 3 slightly decreases. The inverse pole figures for the coating deposited at

500 mTorr show again random orientation of HA crystallites for all three sample directions.

4. Discussion

When considered together, our results indicate that both background pressure and laser energy density have a significant influence on coating texture. Because of the nature of the PLD process, these deposition parameters are strongly coupled. Reduced pressures lead to an increase in the mean free path of the plume species and consequently to a higher kinetic energy of these same species upon deposition. This effect seems to favor stronger texturing of HA grains in the coatings. Low pressure and high laser energy density have a similar effect on the kinetic energy of the plume species and therefore it is likely that the same underlying mechanism of texture formation is responsible for the enhanced texturing effects observed with increasing laser energy density and reduced pressures. Further pressure reduction leads to TTCP formation because of OH insufficiency for HA growth in the coatings. Based on our results, several hypotheses associated with the highly energetic and directional nature of the laser plume can be considered to explain texture development of HA grains in the coatings produced by PLD. In this section, we discuss the two most likely driving forces for texture formation in this system, namely, minimization of strain energy and kinetic effects due to OH transport during coating deposition.

4.1 Stress-induced HA texture and TTCP formation

C-axis texturing in HA may arise due to the anisotropic stress HA experiences during PLD. The direction of the laser plume leads to high values of compressive stress along the deposition direction during growth. This, coupled with the anisotropic elastic modulus of the HA crystals may result in textured polycrystalline configurations that minimize strain energy. Texture formation has been observed in other hexagonal ceramics deposited under anisotropic stress conditions and may be one of the main routes for strain energy relaxation [39]. Since our HA coatings exhibit no residual stress after deposition, as indicated by no detectable changes in peak position and width in XRD scans, it is essential to estimate the magnitude of stresses that may have been present during deposition. If such stresses are found to be significant, this could lend support to the notion that texture is induced by stress. Stresses developed in thin films during deposition can arise from thermal or lattice mismatch between depositing material and substrate, incomplete structural-ordering processes occurring during growth, and interactions between the depositing material and impurities incorporated in the films [40]. For temperatures used in our experiments (650–700 °C), the bulk thermal expansion coefficients for HA and Ti-6Al-4V are 14.6×10^{-6}/°C and 9.8×10^{-6}/°C, respectively, and thus a tensile thermal stress in the 142–153 MPa range is expected for our HA films. Bombardment of the growing film with energetic species commonly leads to compressive stresses within the film. A simple model for the stress tensor experienced by a volume Ω_i of the coating at the position of the i^{th} atom during deposition under bombardment by energetic species may be written as

$$\sigma_i^{\alpha\beta} = -\frac{1}{\Omega_i}\left(\frac{1}{2}\sum_{j\neq i} F_{ij}^{\alpha} r_{ij}^{\beta} + M_i V_i^{\alpha} V_i^{\beta}\right) \quad (1)$$

where r_{ij}^{β} and F_{ij}^{α} are interatomic distances and forces, and M_i and $V_i^{\alpha,\beta}$ are the mass and velocity of depositing species [41]. The first term on the right hand side of Eq. (1) represents the static contribution to the stress tensor, derived from the interatomic forces and relative atomic positions in the depositing material (i.e., contribution from incomplete structural ordering during growth). The term involving $M_i V_i^{\alpha} V_i^{\beta}$ represents the kinetic contribution to the stress during PLD, resulting from the momentum of incoming species. The velocities $V_i^{\alpha,\beta}$ are determined by the kinetic energy and propagation direction of the plume, which in turn depend on laser energy density, background pressure, and plume angle of incidence. This kinetic contribution becomes the dominant term when very high particle velocities are involved. Results from plume diagnostics experiments carried out during PLD of HA allow the estimation of the magnitude of this kinetic contribution. In these experiments the leading edge of the plume is found to be dominated by oxygen atoms (m = 2.68 × 10^{-26} kg) with a speed of 2 × 10^4 m/s for ablation at 2.6 J/cm^2 and 75 mTorr [42]. This speed can be corrected for our experimental conditions (7 J/cm^2 and 600 mTorr) using the classical shock wave model of Zel'dovich and Raizer [43] yielding a speed of 1.6 × 10^4 m/s (21 eV). The total atomic flux in our experiment ranges from 2.1 × 10^{18}/m^2 to 6.5 × 10^{18}/m^2 corresponding to deposition rates of 0.018–0.055 nm/pulse. Using the above speed and range of atomic fluxes, and a penetration depth of approximately 1 nm for 21 eV oxygen ions into HA, as estimated by a SRIM-2003 simulation [44], Eq. (1) can be used to estimate the total kinetic contribution to the stress, which evaluates to 6–19 GPa. These high values of stress are consistent with values predicted by molecular dynamics simulations and measured *in situ* during early stages of highly energetic deposition [45,46]. Estimation of

the static contribution to the stress in Eq. (1) is difficult in our case because we currently do not have access to the atomic configuration in the coatings during deposition. Residual stress in thin films deposited under similar conditions with bombardment by somewhat more energetic species (50–100 eV) tend to be compressive with values in the range of 1–5 GPa [47]. These estimations suggest that in the dynamic deposition conditions involved in our experiment, the kinetic term represents a substantial if not the major contribution to the total stress. Since lattice mismatch, temperature gradients, and other sources of stress such as impurity incorporation are not expected to be significant for our thin coatings, we can reasonably conclude that the kinetic contribution to the stress plays an important role in our configuration. This leads to a strong component of the stress tensor along the direction perpendicular to the substrate when the highly accelerated particles strike the surface. It is in this environment that coating deposition takes place, with HA grains forming from a complex interplay of nucleation and growth processes on the substrate surface or by direct deposition of nano- and micron-scale objects suspended in the ablation plume. Because of the lower compressibility of the *c*-axis of HA [48], it is energetically favorable for HA grains to align this least compressible axis parallel to the direction of maximum stress in order to minimize the elastic strain energy. This scenario is consistent with the data in Figs. 1–7 where increased texturing occurs when high compressive stress along the substrate normal is expected (high laser energy density, low background pressure, and normal plume incidence). However, the microscopic mechanisms for texture development in ceramics under compressive stress are not well understood. The range of deposition temperatures used in our experiments (650–700 °C) may allow a variety of processes of texture formation such as rigid rotation of grains

separated by high-mobility grain boundaries and grain recrystallization under compressive stress [8].

The stress environment described above must be accompanied by efficient incorporation of OH, otherwise TTCP develops in the coatings. The formation of TTCP in HA-rich coatings is not surprising given the close similarity between the TTCP and HA crystal structures. Despite their different space groups, the unit cell dimensions of these two phases suggest a variety of metric fits between their structures (HA: $a = b =$ 9.424 Å, $c = 6.879$ Å, $\alpha = \beta = 90°$, $\gamma = 120°$; TTCP: $a = 7.018$ Å, $b = 11.980$ Å, $c = 9.469$ Å, $\alpha = \gamma = 90°$, $\beta = 90.88°$). Moreover, the positions of calcium and phosphate groups in HA and TTCP imply good chemical fits and possible topotactic transformations between the two. It is conceivable, for example, that TTCP grows epitaxially on pre-existing HA crystallites under dehydroxylating conditions. The development of TTCP with *b*-axis texture on HA coatings that otherwise display preferential *c*-axis orientation is suggestive of epitaxy as projections of the two structures along these axes present one of the strongest epitaxic relationships between them [49]. A topotactic transformation of HA into TTCP upon dehydroxylation is also possible, although it is not likely to be the dominant phenomenon in our coatings as previous studies have shown no conversion of HA into TTCP under the severe dehydroxylation conditions of post-deposition vacuum annealing [37].

It is important to note, however, that the explanations of TTCP *b*-axis texture based on epitaxial growth or topotactic transformations delineated above cannot account for all features of the texture data. A case in point is the observation that HA crystals in coatings containing relatively small amounts of TTCP are often randomly oriented. An

example of this is seen in Figs. 6 and 7 for the sample deposited at 500 mTorr. The XRD pattern for this sample (Fig. 6) and the corresponding inverse pole figure for HA (Fig. 7(d)) show the absence of HA texture when TTCP appears in the coating. Inhibition of texture as a result of secondary-phase inclusions is a common phenomenon in numerous materials systems. It has been well documented for metal matrix composites [50,51], quartz/mica microcomposites [52], and some ceramic compounds [53]. The fact that TTCP inclusions seem to lead to randomly oriented HA in this case suggests that, at least under some conditions, TTCP crystals grow with no crystallographic relationship to HA. This indicates that a significant fraction of TTCP crystals (or their nuclei) may originate in the ablation plume. These TTCP crystallites in the plume could form by nucleation from gas-phase species or from nano- and/or microscale HA particulates that upon ejection from the target (or during flight toward the substrate) undergo dehydroxylation and are converted to TTCP nano- or microcrystals. Since TTCP crystallites formed in the plume would deposit with random orientation, this could explain how the HA texture is disrupted as a result of mixing with a random phase.

4.2 Preferred orientation of HA and OH transport

Preferred orientation of HA may also be related to the role OH groups play in stabilizing the HA structure, the way they are incorporated in the coatings, and their distribution in the HA lattice. Since OH is essential for HA formation, deposition is carried out in an OH-rich environment to compensate for the stoichiometric imbalance of the plume which is easily dehydroxylated during ablation of HA [54]. OH incorporation into the coatings occurs then as OH groups from the background are buried by the

heavier plume species. This pulsed process may lead to the deposition of alternating layers of OH-poor and OH-rich material. Such concentration gradients could drive OH transport in the direction normal to the substrate. Significantly, the HA crystal structure features its OH groups stacked along the *c*-axis with no intervening atoms between adjacent groups. In the presence of a sufficiently strong driving force, this atomic arrangement allows efficient transport of OH along the *c*-axis [54]. This favors the crystallization of HA grains with the *c*-axis aligned in the direction of OH transport. Once formed, aligned crystals may grow faster than crystals with random orientation because OH stacks along the transport direction effectively function as "channels" that facilitate OH diffusion and incorporation into the neighboring regions. Aligned crystals may also undergo less damage under impact by energetic plume species than randomly oriented grains, further contributing to their higher growth rate. This scenario is also consistent with the observations in Figs. 1–7. Increasing laser energy density would lead to more severe dehydroxylation in the plume. Consequently, deposited layers whose constituents originate from the plume interior would have very low OH content. At the same time, increased laser energy density would lead to more efficient burial of OH groups from the background in intervening layers. This could create steeper concentration gradients and enhance OH transport within the depositing coating, leading to increased *c*-axis texturing (Figs. 1–3). Departure from normal incidence reduces the component of the plume momentum normal to the substrate, which would decrease the plume-driven incorporation of OH. This would result in milder concentration gradients, less OH transport, and consequently less texturing (Figs. 4 and 5). At large angles of incidence one would expect formation of TTCP inclusions or TTCP growth because of poor OH

incorporation. Lower background pressure results in higher plume kinetic energy. Within a pressure range that guarantees sufficient supply of OH groups, reduced pressures could lead to improved OH incorporation and more texture development (Figs. 6 and 7, 800–600 mTorr). Below a certain pressure one would expect the OH supply to become insufficient for complete hydroxylation of the coating, leading to formation of TTCP (Figs. 6 and 7, < 600 mTorr).

5. Conclusions

We have studied the crystallographic orientation of HA polycrystalline coatings deposited by PLD. High laser energy density and normal incidence of the laser plume lead to HA coatings whose grains have the *c*-axis preferentially aligned perpendicularly to the substrate. This preferred orientation is probably caused by the high compressive stress along the normal to the substrate during PLD and the anisotropic elastic modulus of the HA crystals. OH transport effects during deposition may also play a role in the formation of oriented crystals. Although both scenarios provide reasonable explanations for texture formation in our samples, the relative importance of these processes remains unclear. *In-situ* stress measurements, decoupling of the effect of secondary phase formation, cross-sectional imaging of grain morphology, and atomistic simulations of OH transport in HA may help clarify these processes and suggest alternative mechanisms. These findings may be relevant in the controlled fabrication of textured HA coatings with improved mechanical properties and tailored bioactivity for biomedical applications.

Acknowledgements

This research was supported by the National Institute of Dental and Craniofacial Research (NIDCR) under Grant No. R01 DE013952-04 and by a Major Research Instrumentation award from the National Science Foundation (NSF) under Grant No. DMR-0116098. The authors would like to thank Mr. Jason Wolf at Carnegie Mellon University (CMU) for his assistance with X-ray pole figure measurements. The experiments at CMU were supported by the MRSEC program of the NSF under Award Number DMR-0520425.

References

[1] Solas DE, Tome CN, Engler O, Wenk H-R. Acta Mater 2001;49(18):3791.

[2] Hasegawa M, Yamamoto M, Fukutomi H. Acta Mater 2003;51(13):3939.

[3] Okolo B, Lamparter P, Welzel U, Wagner T, Mittemeijer EJ. Thin solid films 2005;474(1):50.

[4] Bruhn DF, Casey M. J Struct Geol 1997;19(7):909.

[5] Neumann B. J Struct Geol 2000;22(11-12):1695.

[6] Mizukami T, Wallis SR, Yamamoto J. Nature 2004;427(6973):432.

[7] Kocks UF, Tomé CN, Wenk H-R. Texture and anisotropy. Cambridge University Press:1998.

[8] Bunge HJ. Textures Microstruct 1991;14-18:283.

[9] Wenk H-R, Phillips D. Physica C 1992;200:105.

[10] Ohyama M, Kozuka H, YoKo T. J Am Ceram Soc 1998;81:1622.

[11] Heydt P, Luo C, Clarke DR. J Am Ceram Soc 2001;84:1539.

[12] Denry IL, Baranta G, Holloway JA, Gupta PK. J Biomed Mater Res 2002; 64B: 70.

[13] Mukherjee S, Prokert F, Richter E, Moeller W. Surf Coat Technol 2004;186:99.

[14] Fujito G, Wakiya N, Kiguchi T, Mizutani N, Shinozaki K. Key Eng Mater 2006;320:65.

[15] Hall DA, Steuwer A, Cherdhirunkorn B, Mori T, Withers PJ. J Appl Phys 2004;96:4245.

[16] Hall DA, Steuwer A, Cherdhirunkorn B, Mori T, Withers PJ. Acta Mater 2006;54:3075.

[17] Dawber M, Rabe KM, Scott JF. Rev Mod Phys 2005;77:1083.

[18] Alkoy EM, Uchiyama K, Shiosaki T, Alkoy S. J Appl Phys 2006;99:106106.

[19] Lenoir B, Scherrer H, Caillat T. in Recent Trends in Thermoelectric Materials Research I, Semiconduct Semimet 2001;69:101.

[20] Teichert S, Sarkar DK, Schwendler S, Giesler H, Mogilatenko A, Falke M, Beddies G, Hinneberg HJ. Microelectron Eng 2001;55:227.

[21] Vereecken PM, Ren S, Sun L, Searson PC. J Electrochem Soc 2003;150:C131.

[22] Wenk H-R, Heidelbach F. Bone 1999;24(4):361.

[23] Nakano T, Kaibara K, Tabata Y, Nagata N, Enomoto S, Marukawa E, Umakoshi Y. Bone 2002;31(4):479.

[24] Sasaki N, Ikawa T, Fukuda A. J Biomech 1991;24(1):57.

[25] Roeder RK, Sproul MM, Turner CH. J Biomed Mater Res 2003;67A:801.

[26] Hench LL, Wilson J. An introduction to bioceramics. World Scientific:1993.

[27] de Groot K. Mater Technol 1993;8:12.

[28] Cotell CM, Chrisey DB, Grabowski KS, Sprague JA, Gossett CR. J Appl Biomater 1992;3:87.

[29] Tong W, Chen J, Li X, Feng J, Cao Y, Yang Z, Zhang X. J Mater Sci 1996;31:3739.

[30] Roome CM, Adam CD. Biomater 1995;16(9):691.

[31] van Dijk K, Schaeken HG, Wolke JCG, Maree CHM, Habraken FHPM, Verhoeven J, Jansen JA. J Biomed Mater Res 1995;29:269.

[32] Kawasaki T. J Chromatogr 1991;544:147.

[33] Kim H, Vohra YK, Lacefield WR, Camata RP. Mater Res Soc Sym Proc 2003;750:71.

[34] Kim H, Vohra YK, Louis PJ, Lacefield WR, Lemons JE, Camata RP. Key Eng Mater 2005;284–286:207.

[35] Watanabe Y, Ikoma T, Monkawa A, Suetsugu Y, Yamada H, Tanaka J, Moriyoshi Y. J Am Ceram Soc 2005;88(1):243.

[36] Fernández-Pradas JM, Sardin G, Clèries L, Serra P, Ferrater C, Morenza JL. Thin Solid Films 1998;317:393.

[37] Kim H, Camata RP, Lacefield WR, Vohra YK. J Mater Sci Med 2005;16:961.

[38] Kallend JS, Kocks UF, Rollett AD, Wenk H-R. Mater Sci Eng A 1991;132:1.

[39] Gan BK, Bilek MMM, McKenzie DR, Taylor MB, McCulloch DG. J Appl Phys 2004;95(4):2130.

[40] Nalwa HS. Handbook of thin film materials. Academic Press:2002.

[41] Smith RW, Srolovitz DJ. J Appl Phys 1996;79(3):1448.

[42] Serra P, Morenza JL. J Appl Phys 1999;85(6):3289.

[43] Zel'dovich YB, Raizer YP. Physics of Shock Waves and High Temperature Hydrodynamic Phenomena vol.1. Academic Press:1996. p. 94.

[44] Ziegler JF. Nucl Instrum Meth B 2004;219:1027.

[45] Bilek MMM, McKenzie DR. Surf Coat Technol 2006;200:4345.

[46] Carneiro JO, Teixeira V, Portinha A, Vaz F, Ferreira JA. Rev Adv Mater Sci 2004;7:32.

[47] Davis CA. Thin Solid Films 1993;226:30.

[48] Velisavljevic N, Vohra YK. Appl Phys Lett 2003;82:4271.

[49] Dickens B, Brown WE, Kruger GJ, Stewart JM. Acta Cryst 1973;B29:2046.

[50] Poudens A, Bacroix B, Bretheau T. Mater Sci Eng A 1995;196:219.

[51] Wassermann G, Bergmann HW, Frommeyer G. Textures of materials. Springer:1978.

[52] Tullis J, Wenk H-R. Mater Sci Eng A 1994;175:209.

[53] Sintubin M, Wenk H-R, Phillips DS. Mater Sci Eng A 1995;202:157.

[54] Manso M, Herrero P, Fernández M, Langlet M, Martínez-Duart JM. J Biomed Mater Res 2003;64A:600.

Figure captions

Fig. 1. X-ray diffraction scans for coatings deposited at 600 mTorr and 650 °C with different laser energy densities of 5 J/cm^2, 6 J/cm^2, and 7 J/cm^2. Indexed peaks represent hydroxyapatite reflections. Reflections marked with a cross (+) are from the Ti-6Al-4V substrate. The broad feature marked by an open circle (o) is ascribed to CaO.

Fig. 2. X-ray pole figures for the hydroxyapatite $\{0001\}$ and $\{1\bar{2}1\}$ poles for coatings deposited at 600 mTorr and 650 °C with different laser energy densities. The axes 1 and 2 (see inset) represent the directions parallel to the film surface whereas the axis 3 indicates the direction perpendicular to the coating surface. The intensities are expressed in units of multiples of random distribution (MRD).

Fig. 3. Inverse pole figures for hydroxyapatite in coatings deposited at 600 mTorr and 650 °C with different laser energy densities, corresponding to the pole figure data displayed in Fig. 2. The intensities are expressed in units of multiples of random distribution (MRD).

Fig. 4. X-ray diffraction scans for coatings deposited at 600 mTorr and 650 °C with a laser energy density of 7 J/cm^2 at different angles of incidence of the ablation plume. Indexed peaks correspond to hydroxyapatite reflections while peaks marked by an asterisk (∗) originate from tetracalcium phosphate. (o: CaO).

Fig. 5. Inverse pole figures for hydroxyapatite in coatings deposited at 600 mTorr and 650 °C with a laser energy density of 7 J/cm^2 for angles of incidence of the plume $\varphi = 0°$ and $\varphi = 15°$. Inverse pole figures for $\varphi > 15°$ were not generated due to overlap of the hydroxyapatite (0002) and tetracalcium phosphate (130) peaks.

Fig. 6. X-ray diffraction scans for coatings deposited at 650 °C with a laser energy density of 6 J/cm^2 and normal incidence of the plume for various pressures of the Ar/H_2O background atmosphere. Reflections marked with a cross (+) are from the Ti-6Al-4V substrate. (∗: tetracalcium phosphate; o: CaO).

Fig. 7. Inverse pole figures for hydroxyapatite in coatings deposited at 650 °C with a laser energy density of 6 J/cm^2 and normal incidence of the plume for various pressures of the Ar/H_2O background atmosphere. Inverse pole figures for pressures below 500 mTorr were not generated due to overlap of the hydroxyapatite (0002) and tetracalcium phosphate (130) peaks.

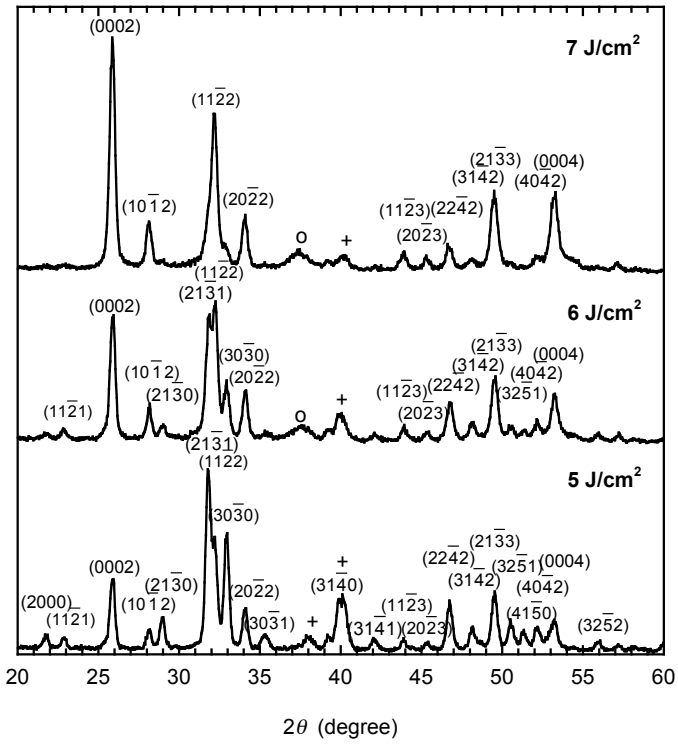

Fig. 1., Kim et al.

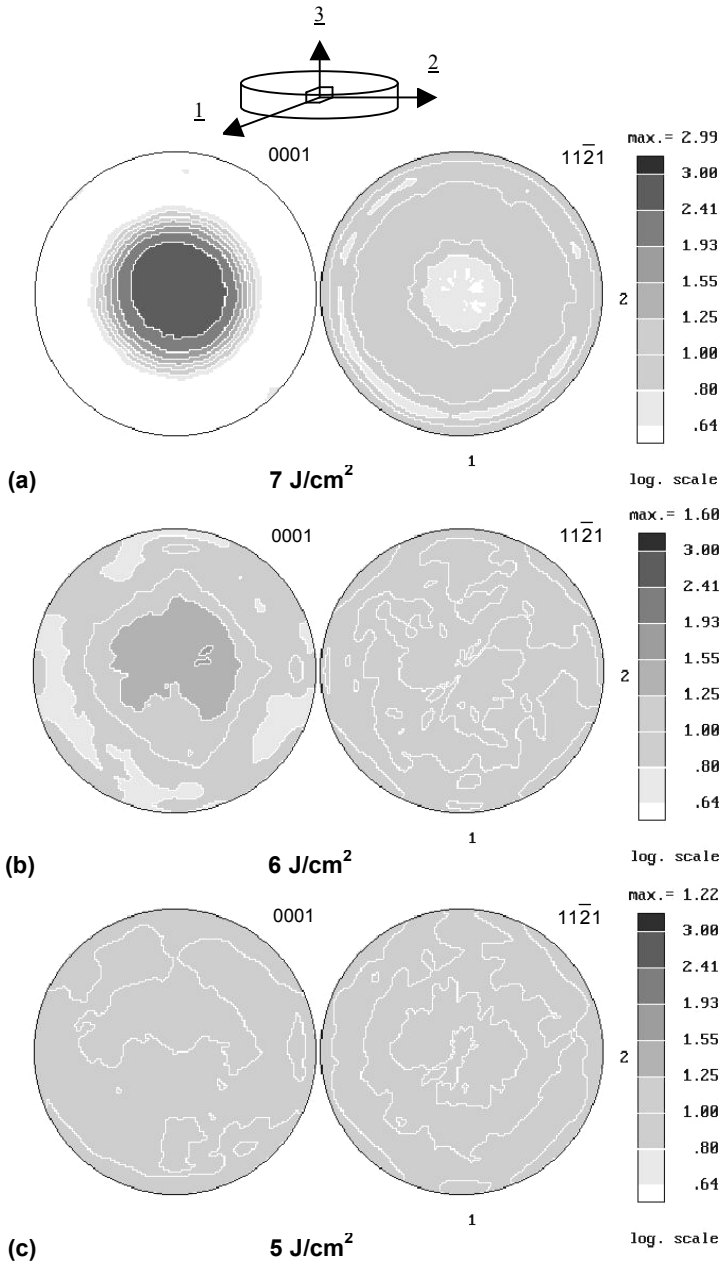

Fig. 2., Kim et al.

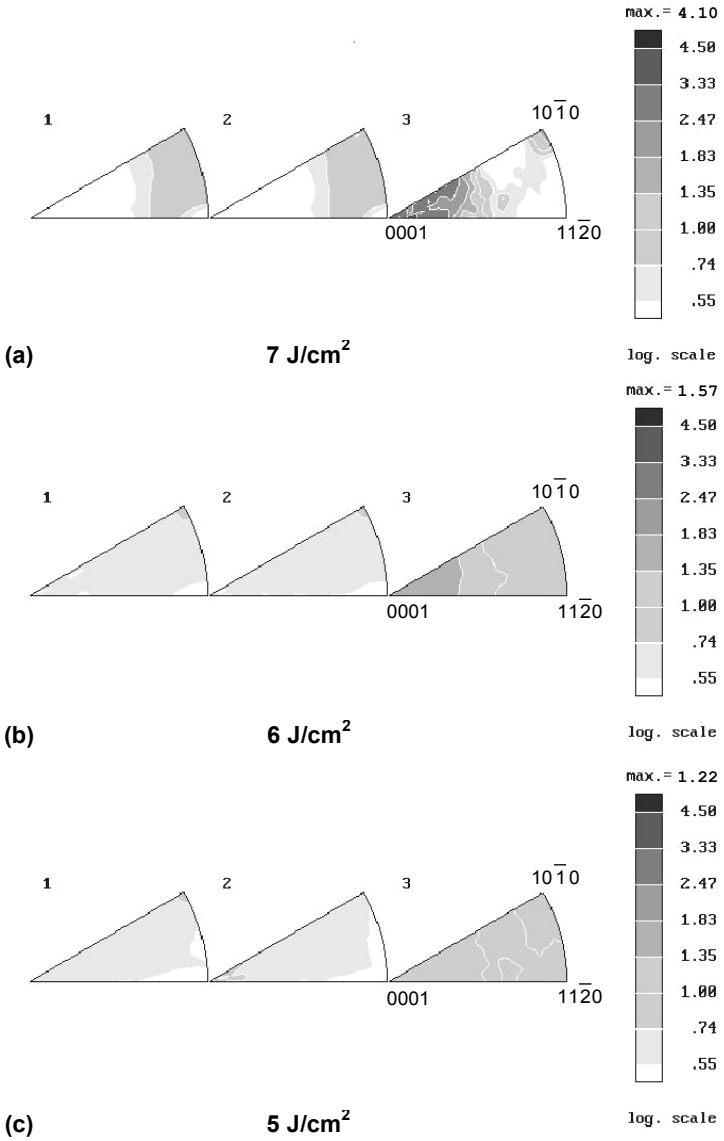

Fig. 3., Kim et al.

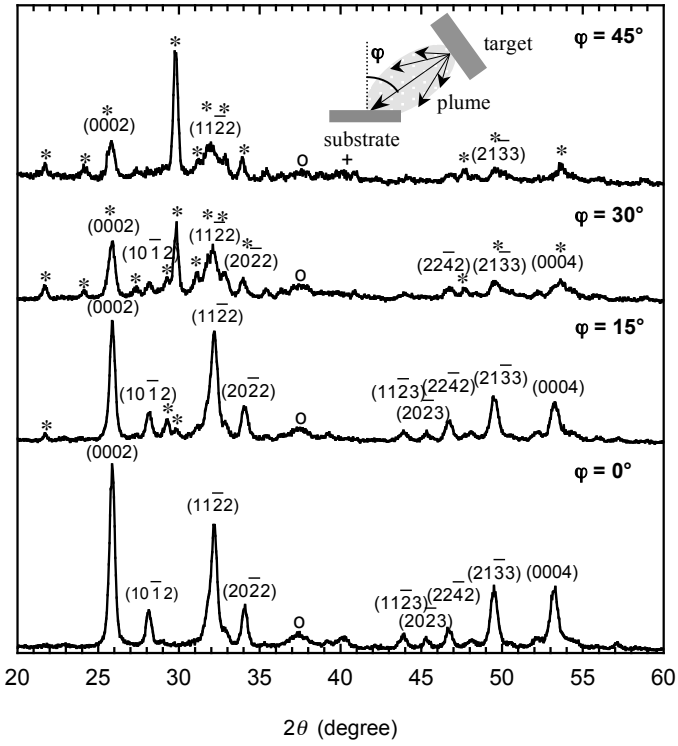

Fig. 4., Kim et al.

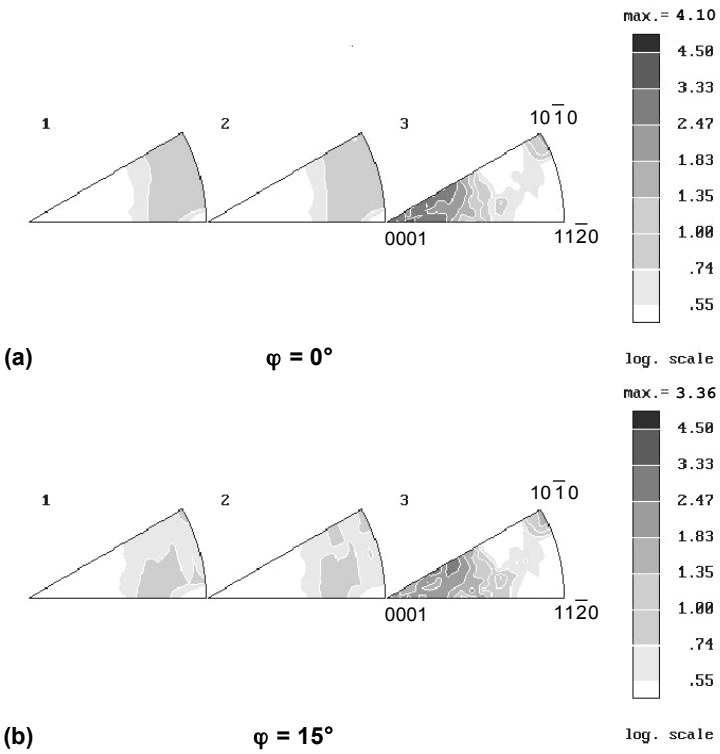

Fig. 5., Kim et al.

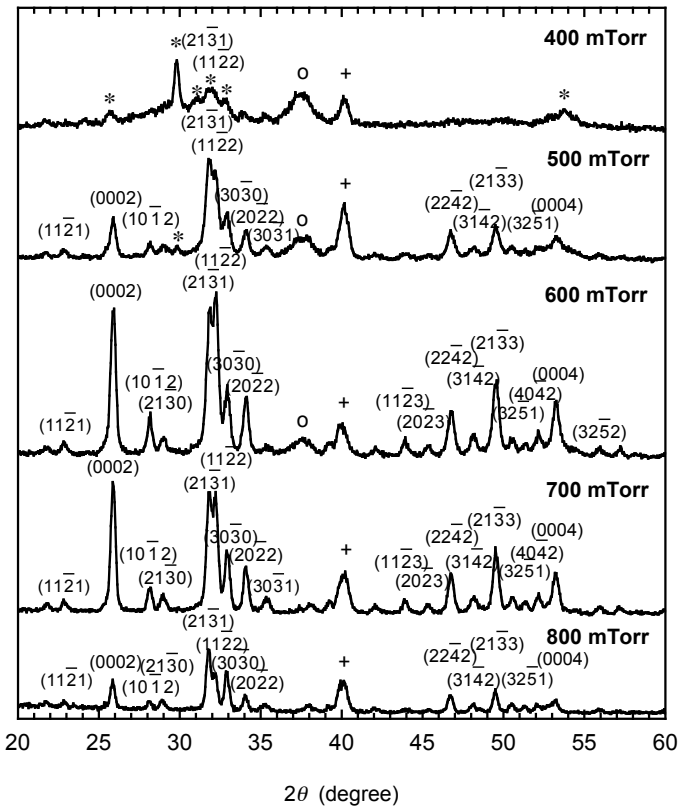

Fig. 6., Kim et al.

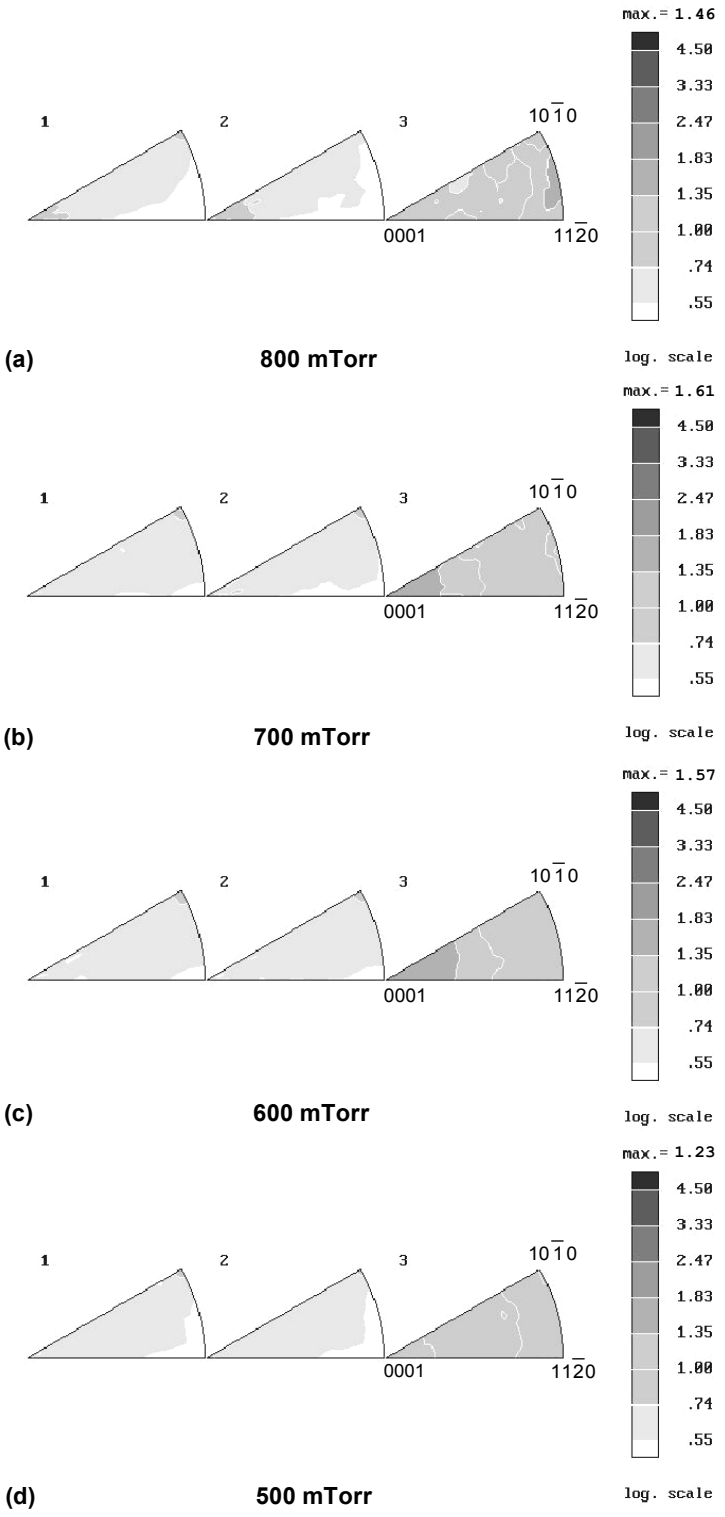

Fig. 7., Kim et al.